Fatigue fracture assessment of 10CrNi3MoV welded load-carrying cruciform joints considering mismatch effect

Wei Song[1,*], Xuesong Liu[2], Jie Xu[3], Yu Fan[3], Duanhu Shi[1], Min He[1], Xiaoxi Wang[1], Filippo Berto[4]

1. School of Mechanical & Electrical Engineering, Xuzhou University of Technology, Xuzhou 221018, PR China.

2. State Key Laboratory of Advanced Welding and Joining, Harbin Institute of Technology, Harbin 150001, China.

3. School of Materials Science and Physics, China University of Mining and Technology, Xuzhou, 221116, PR China.

4. Department of Mechanical and Industrial Engineering, Norwegian University of Science and Technology (NTNU), Richard Birkelands Vei 2b, 7491 Trondheim, Norway.

Abstract:

Fatigue experiments and numerical simulations based on the Linear Elastic Fracture Mechanics (LEFM) theory were conducted on the Even-Matched (EM) and Under-Matched (UM) 10CrNi3MoV Load-carrying Cruciform Welded Joints (LCWJs). The study firstly experimentally investigated the Fatigue Crack Growth Rate (FCGR) of base metal, EM, and UM weldments. The corresponding Paris parameters as essential input data are provided to assess the fatigue crack propagation behavior for weld toe and weld root failure of LCWJs. On the one hand, the Stress Intensity Factors (SIFs) at weld toe and weld root were calculated considering the effects of LCWJ specimen geometries, initial crack types, and sizes. The comparisons between simulated results and standards analytical solutions were executed, which exhibit good accordance. It proved that the fatigue fracture simulation procedure based on LEFM is appropriate for the fatigue assessment of LCWJs. Eventually, it conducted the parametric analysis by predicted S-N curves, which included in the weld length, initial crack shape, initial crack size, penetration length, and materials fracture parameter, to explore some safety assessment reference lines for both failure modes of LCWJ.

Nomenclature:

a, crack length; α, notch opening angle; BM, Base Metal; CT, Compact Tension; e_i, parameters dependent on the opening angle; $\Delta\sigma_n$, remotely applied stress; E, Young's modulus; ETS, Effective Traction Stress; EETS, Equivalent Effective Traction Stress; FE, Finite Element; FEA, Finite Element Analysis; FCGR, Fatigue Crack Growth Rate; H, leg length; h, weld size; K_i, stress intensity factors; L, attachment plate thickness; LCWJ, Load-carrying Cruciform Welded Joints; LEFM, Linear Elastic Fracture Mechanics; MTS, Maximum Tangential Stress; M, crack state; NSIF, Notch Stress Intensity Factor; PSM, Peak Stress Method; p, lack of penetration; q, geometry parameter; R_c, radius of the semicircular sector; SED, Strain Energy Density; SERR, Strain Energy Release Rate; θ, the kink angle; σ_m, membrane stress; σ_b, bending stress; t, the plate thickness; Y, structural geometry; v, Poisson's ratio; w_i, non-dimensional parameters; PWHT, Post Welding Heat Treatment; W_i, weld number; WM, Weld Metal.

Keywords:

1. Introduction

Welding is one of the most important joining technologies in various industries, such as shipbuilding, offshore installations, bridges, and engineering machinery, etc. The load-carrying cruciform welded joint is widely used to connect different plate components. It is inevitable to occur some no- or partial penetration, which causes fatigue cracks initiating from the notch tip of weld toes or roots. The variation of length of penetration can change the load-carrying section, further influence the load-carrying capability and even the joints failure mode (Failure from weld toe or weld root). According to the definition of fatigue resistance S-N curves for steel in IIW recommendations [1], this transition of failure mode ultimately results in a sharp decrease of fatigue class from medium FAT 63 to lowest FAT 36. It means that the fatigue life associated with weld root failure in LCWJs is significantly shortened compared with that weld toe failure under the same loading condition. Such failure mode can be attributed to the various forms of defects surrounding weld root and inherent variability in weld throat size and weld penetration[2,3].

Fatigue assessment approaches have been widely developed for different engineering fields and numerous welded structures. In the codes mentioned above, the recommended nominal, structural hot-spot, and effective notch stress approaches regard different types of stress as fatigue governing parameters to characterize a critical failure point of welded joints. Additionally, some new structural approaches and local approaches using related governing parameters, such as the Equivalent Effective Traction Stress (EETS) method [4], Notch Stress Intensity Factor (NSIF) method[5], and Strain Energy Density (SED) method [6] which is extended from NSIF method, peak stress (PSM) method [7] orientated from SED method, are also used to evaluate fatigue failure behavior and predict fatigue life validly. Aiming at the initiation of weld toe or weld root fatigue failure, accuracy estimation of fatigue life not only needs to choose appropriate assessment approach but also to judge available failure locations of welded joints. Xing and Dong [8] established analytical solutions by EETS method to determine failure mode transition and critical weld size of LCWJs taking into account of weld penetration and joints misalignment; the results are shown to agree well with the amount of experiments data. Due to the unit discrepancy of different notch angles in Williams' notch theory, NSIF governing parameter cannot compare weld toe and weld root failure location simultaneously. Because the relationship between weld toe failure and weld root failure in LCWJs was further investigated by an alternative SED approach in [9]. The results based on the SED approach predicted precisely the transition region comparing with test data. According to the above researches of quantitative weld size, the weld root failure mode of LCWJs can be effectively prevented with a clear boundary. Although the minimum fillet weld size with a confidence level can be determined to ensure that fatigue failure location would not occur in weld root, limited literature has studied the disparity of fatigue life between weld

toe failure and weld root failure quantitatively. Since fatigue cycle numbers cannot be predicted by the above assessment approaches.

In general, the fatigue life of metallic materials and structures includes crack initiation and crack propagation stages. For notched members, the fatigue life of these components without any initial cracks under cycle fatigue loading is dominated by crack initiation, which is dependent on notch severity[10]. However, the existence of crack-like imperfections in welded joints will decrease cycles of crack initiation stage, and most of fatigue life of welded joints is spent in crack propagation stage. Crack initiation life of welded components is only a small portion of total fatigue life, which can be neglected in practical engineering applications[11], especially for the cases of welded joints with incomplete penetration. Therefore, the fatigue assessment for welded structures should be focused on the fatigue life of the crack growth portion, which can be evaluated within the framework of linear elastic fracture mechanics (LEFM). According to the instructions of international codes, such as IIW [1], BS7910 [12], and Eurocode 3 [13], they recommend related initial crack shape and size for different welded joints. When the position of crack initiation is determined by actual joints geometry and failure transition size criteria, the SIF with stable macroscopic crack growth from the initial location can be calculated under cyclic loading. For obtaining a conservative fatigue strength, the force-controlled tensile loading was applied [14]. Thus, the crack propagation fatigue lives for weld toe and weld root failure modes can be calculated by combining accurate stress intensity factors with related materials Paris law parameters.

Associated codes and recommendations on the basis of LEFM have been established to guide the fatigue assessment of welded components, such as initial crack size (0.1mm), initial aspect ratio (1), initial crack size set as min(t/2) and exponent of Paris-Erdogan power law (m=3) [1]. C. Fischer and W. Fricke[15] performed 2D crack propagation analysis into three specimen types (U-notch joint, cruciform joint, T joint) with cracks using real material parameters from Maddox. The computed crack propagation life agreed very well with experimental data and further confirmed that the fracture mechanics approach was reliable to estimate the fatigue life of welded joints. For the welded joints with high-stress peaks, crack propagation investigation considering the crack shape at plate corner cannot interpret the experiment phenomenon from the difference of crack growth speed between the corner crack located in steep stress gradient point and surface semi-elliptical crack [16].

In light of the effect of crack shape on fatigue performance of non-load-carrying cruciform joints taking account of 3D mix-mode fracture, four types of initial crack shape (line crack, line cold lap, semi-elliptical crack, semi-elliptical cold lap) were assumed to give a comparison among fatigue life predicted results by Zong et al.[17]. The results suggest that the line cold lap assumption with 0.1mm initial crack size can give a satisfied estimation by comparing with experimental data. Furthermore, 0.01mm initial line crack assumption for I-type crack provides better-predicted results according to the lower bound of the S-N curve with a 95% survival probability. A similar fatigue behavior investigation of bridge weathering steel Q345qDNH non-load-carrying cruciform joints was conducted by experimental and simulation methods [18]. It is recommended to adopt a semi-elliptical crack with an initial crack depth of 0.075 mm for numerical simulation when the initial crack size is unknown. Regarding LCWJs, multi-crack analysis considering weld failure toe and weld root failure modes was studied [19]. They proposed that the 0.5mm weld toe and 0.1mm weld root initial line crack can be suitable for the prediction of fatigue life. However, these

analyses of failure mode only aim at specific weld joints size. Details of the fracture mechanics approach and the applications in terms of fatigue failure issues for different types of welded joints and components were exhibited in [20-28], including the model extension for specific welded joints, residual stress effect, failure mode effect, geometry differences, and loading modes et. al. It still needs further investigation of the relationship between specimen geometry variation and fatigue crack propagation life. An accurate characterization of LCWJs geometry, crack propagation and crack growth parameters of HAZ/BM materials are necessary when we employ the fracture mechanics theory to describe the propagation process from an initial crack to final failure.

The current study is concerned with the fatigue behaviors of LCWJs under cyclic tensile loading by LEFM theory. We start with the investigation of initial crack types and weld geometry (weld length and penetration) on SIFs for LCWJ different failure modes by comparing the numerical simulation results and analytical solutions in standards. Under given weld length and penetration, the failure mode of weld toe or weld root can be determined by SIFs comparison between critical weld size and actual weld geometry. Subsequently, fatigue life is quantitatively estimated by fracture mechanics analysis according to specific failure mode and different Paris material fracture parameters. Finally, the fatigue life predictions considering various factors on which influences fatigue crack propagation, such as failure modes, FCG of materials, defeats types, and the size of defeats, are estimated. The suitable initial crack assumptions for both weld toe and weld root failures in LCWJs are determined.

2. Materials and experimental procedures

2.1 Materials

The high strength steel 10CrNi3MoV investigated in this study is employed in the shipbuilding industry due to the excellent strength and plasticity. The nominal chemical composition of base metal, corresponding evenmatched weldments, and undermatched weldments from the manufacturer's certificate are given in [29]. Since the similarity of chemical composition between evenmatched weldments and base metal, we assumed that the mechanical properties of base metal and evenmatched welds are the same. 10CrNi3MoV high strength low alloy steel, which is quenched and tempered, has a fine microstructure mainly composed of acicular ferrite and granular carbides. The basic mechanical properties and low cycle fatigue results were also given in [29]. It should be noted that the undermatched ratio for LCWJs is about 0.72. The low cycle fatigue investigation and related results have published in [29].

2.2 Fatigue crack growth tests

The experimental investigation includes FCGR tests and LCWJs fatigue tests in order to obtain relative fatigue crack propagation parameters of material and fatigue life of welded specimens. The materials used in the fatigue crack growth and fatigue tests of welded cruciform joints are 10CrNi3MoV steels, which are widely used in the fabrication of ship-building structures.

Multi-pass butt-welding and fillet welding were conducted on different grooved plates with 10mm thickness plates using the Gas Metal Arc Welding (GMAW) procedure.

A schematic illustration of Compact Tension (CT) specimen orientation and the extraction location of the welded region is shown in Fig. 1(a). CT specimen dimensions were designed following the ASME E647 standard, which was shown in Fig. 1(b). The specimen thickness B was 10mm. The FCG specimens were sampled from the welded plate along the welding direction and labeled based on the material microstructure (i.e., BM and WM). As for the CT specimens of weldments, the notches were manufactured along the center of the butt welds. It is worth to note that no post-weld heat treatment (PWHT) was performed on CT specimens to replicate the real as-welded state. Before testing, the samples were fatigue pre-cracked according to the specific procedure. A lower bound threshold stress intensity factor range between 10 and 12 MPa·m$^{0.5}$ was used to initiate the crack from the notch. Then a decreased 5% ΔK value was set stepwise until it reached the target K value. Typically, the pre-cracks were processed about 2 mm for these materials.

The CMOD measuring system on the basis of the compliance method is applied to obtain the FCG rates by accessional fracture extensometer. The theoretical expression of the compliance method is illustrated explicitly in the ASTM E647-15 standard [30]. The FCGR loading equipment is a servo-hydraulic Instron 8802 machine. The load capacity of the device is 25 tons for both tension and compression. All the FCGR tests are performed under a frequency of 10 Hz under a stress ratio of R = 0.1.


(a) Schematic diagram of CT specimens from welded plate

(b) Geometry of CT specimens
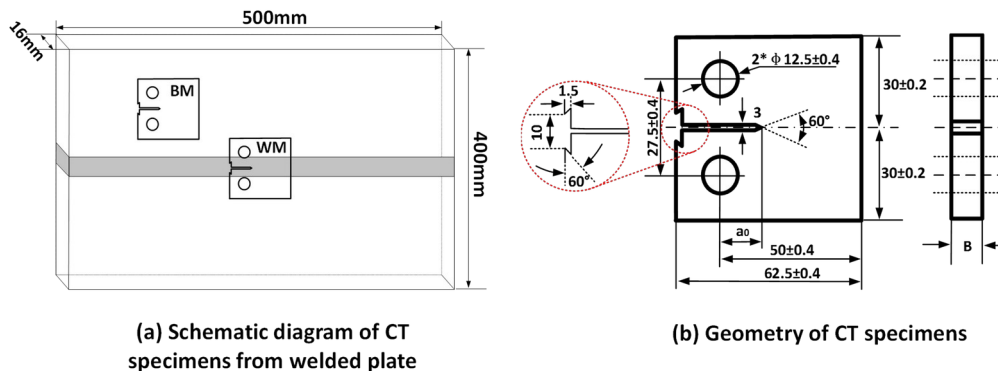
Fig. 1 Geometry schematic of the weld plate and CT specimens

2.3 Fatigue tests of LCWJ

Typical LCWJs were investigated in our study. Welded joints components were first fabricated from two 500mm*150mm*10mm plates and one stiffening plate by the GMAW method, as shown in Fig. 2(a). Then welded components were cut into cruciform welded joints (Fig. 2(b)) with width 50mm by electrical discharge machining. To observe the fatigue crack growth conveniently, the surface of these specimens was polished by sandpapers. The high cycle fatigue tests of LCWJs were carried on a 250KN electro-hydraulic servo testing system MTS 809 under force-controlled condition (see Fig. 2(c)). Before fatigue testing, specimen geometry dimensions, including welds length and welds penetrations, were measured and examined for each specimen by image processing method, as shown in Fig.2(d) and (e). The nominal stress

range of 100-200 MPa was loaded with a stress ratio (R=0.1) and loading frequency between 5 and 15Hz. Fig .2 (f) displayed the final fatigue failure modes. The geometrical details of welded joints and related high cycle fatigue test results were summarized in [31].
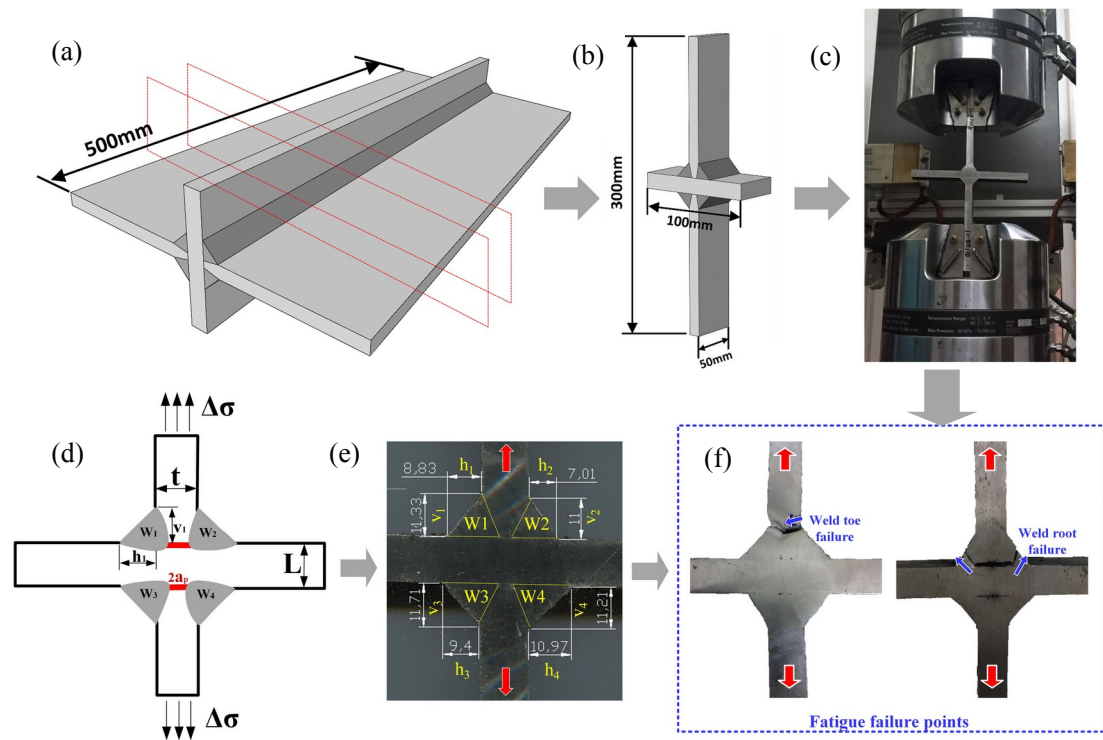

Fig. 2 Load-carrying cruciform joints geometric and test details. (a) Load-carrying cruciform plate, (b) cutting specimens geometry, (c) fatigue tests, (d) Joints geometric illustration, (e) Joints geometric measurement, (f) fatigue failure modes. [27]

3. Tests results and observations

3.1 Fatigue crack growth rates

Fatigue crack growth rate tests on base metal and weldments were performed at room temperature. Generally, stage II fatigue crack growth domain was quantitively described by the Paris law:

$$da / dN = C \cdot \Delta K^{m} \tag{1}$$

Where a represents the crack length, and N is the number of the cycles, giving da/dN the discrete crack extension/growth per cycle. C and m are constants related to material and testing conditions, while ΔK is the range of the SIF experienced by the material during the fatigue cycles. The ΔK ranges in the measuring machine are calculated using the formula proposed in ASTM E647 for CT specimens:

$$\Delta K_{I} = \frac{\Delta P}{B\sqrt{W}} \cdot \frac{(2+\alpha)}{(1-\alpha)^{3/2}} \left(0.886 + 4.64\alpha - 13.32\alpha^{2} + 14.72\alpha^{3} - 5.6\alpha^{4} \right) \tag{2}$$

Where α= a/W, a is the crack size, B is the thickness of the specimen, W is the width of the

sample, and ΔP is the applied load range. As for the crack growth rate da/dN, it can be computed using the seven-point incremental polynomial technique also recorded in the ASTM E647 standard. Furthermore, regression analysis is conducted under logarithmic coordinates, and FCGR parameters in terms of Paris' law can be derived by the computed da/dN and ΔK. The FCGR curves of base metal and weldments are given in Fig. 3. BM, E-WM, and U-WM represent base metal, evenmatched weldments, and undermatched weldments, respectively.
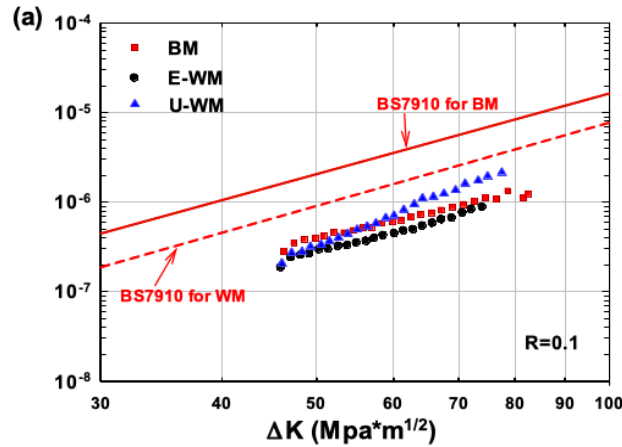
Fig. 3 FCGR tests results including base metal and weldments

Some FCGR design codes in terms of Paris law have been included in BS7910 and IIW for base metal and weldments. The related parameters for different units are presented in table 3. As shown in this table, the values of C for the base metal in IIW are less than that for weldments under the same units, which means FCGR of base metal is lower than that of weldments. Meanwhile, the referred parameters of Paris law from BS7910 and IIW are the difference. The FCGR results of steel in IIW is higher than that in BS7910, while the FCGR of weldments in IIW is lower than that in BS7910. To avoid unreliable assessment of fatigue crack behavior, we compared the experimental data with the BS7910 standards herein.

In Fig. 3, it is shown that base metal of 10CrNi3MoV steel has a higher FCGR than E-WM and U-WM below ΔK value of 58 $MPa \cdot m^{1/2}$. Above this magnitude, test data of base metal are lower than E-WM and U-WM. However, the FCGR for all test results is more moderate than BS7910. It is demonstrated that 10CrNi3MoV steel and its weldments have excellent fatigue resistant capacity. The related Paris law parameters of materials fitting from FCGR tests are summarized in Table 1.

Table 1. Referred parameters of Paris law in standards and test materials.

	Material	Environment	Units	C	m
IIW(2016)	Steel (BM)	Air	N and mm	3×10⁻¹³	3
	Steel (BM)	Air	N and m	9.487×10⁻¹²	3
	weldment	Air	N and mm	5.21×10⁻¹³	3
	weldment	Air	N and m	1.647×10⁻¹¹	3
BS7910	Steel (BM)	Air	N and mm	5.21×10⁻¹³	3
	Steel (BM)	Air	N and m	1.65×10⁻¹¹	3
	weldment	Air	N and mm	1.10×10⁻¹³	3.1
	weldment	Air	N and m	4.91×10⁻¹²	3.1
Test	BM	Air	N and mm	1.24×10^{-11}	2.65

materials	E-WM	Air	N and mm	2.13×10^{-13}	3.49
	U-WM	Air	N and mm	4.74×10^{-14}	4.01

3.2 Fatigue life data of LCWJ

All valid high cycle fatigue test data for different failure modes (weld toe and weld root) were depicted in the logarithmic coordinate system in Fig. 4. It can be found that the fatigue life data (solid red circle) of weld root failure is significantly shorter than that of weld toe failure (blue square), which is also verified in other references[19,23]. However, it is no noticeable difference in high cycle fatigue life data between evenmatched and undermatched welds. It further illustrated that weldments' strength mismatch makes no difference in the high cycle fatigue life of LCWJs.

On the other hand, the related fatigue life recommendations from different standards (IIW, BS7608, DNV-RP-C203, EuroCode3 (EC3), JSSC, and ASME) are summarized in Table 2. According to the comparison of these standard codes, it shows the same S-N reference line (FAT36 under $N_f=2\times10^6$ cycles) for fatigue root failure of LCWJ. Regarding the fatigue toe failure of LCWJ, however, the EC3 gives a higher design reference S-N curve (FAT80 under $N_f=2\times10^6$ cycles) than other standard codes. In the IIW standard, the design S-N curve of weld toe failure is FAT63 with the slope of 3. If the EC3 design S-N reference line (FAT80/3) was used for fatigue toe failure assessment, most of the fatigue data could be covered by the line except four points of undermatched welded joints in Fig. 4. Some fatigue test data is not satisfied with the EC3. The test results demonstrate that the EC3 design curves are not suitable for UM LCWJ specimens. Nevertheless, the IIW codes can meet all the fatigue data for different failure modes. From the perspective of the whole welding process, the quality control demand by EC3 seems to be stricter and more reliable [19]. It is also shown in Fig. 4 that the design curves for different failure modes can cover corresponding fatigue test data by the IIW design lines. It proves that the IIW design curves are generally safe and suitable for 10CrNi3MoV steel weldments. Given the effectiveness of fatigue data under different failure modes by observation, it is feasible to choose the IIW codes to assess the fatigue life of LCWJ. Finally, the design S-N curves of IIW and other standards for weld toe failure and weld root failure in LCWJs was also presented in Fig. 4.

Table 2. Fatigue life recommendations from different standards.

Standards	LCWJ	m	logC	FAT(MPa), S_t	Class
IIW	weld toe	3	11.02	63 ($N_f=2\times10^6$ cycles)	
	weld root	3	10.97	36 ($N_f=2\times10^6$ cycles)	
BS7608	weld toe (Full penetration)	3	12.237	40 ($N_f=1\times10^7$ cycles)	F
	weld toe (Part penetration)	3	12.09	35 ($N_f=1\times10^7$ cycles)	F2
	weld root (mode I)	3	11.398	21 ($N_f=1\times10^7$ cycles)	W1
	weld root (mode II or/and III)	5	16.597	37 ($N_f=1\times10^8$ cycles)	S2
DNV-RP-C203	weld toe (full or	3	11.398	29.24 ($N_f=1\times10^7$ cycles)	G

	part penetration)				
	weld root	3	10.97	21 (N_f=1×10^7 cycles)	W3
Eurocode 3	weld toe	3		80 (N_f=2×10^6 cycles)	Category 80
	weld root	3	10.97	36 (N_f=2×10^6 cycles)	Category 36
JSSC	weld toe/root	2.7	11.95	50 (N_f=5×10^6 cycles)	F
ASME	weld toe	2.7		25.9 (N_f=1×10^6 cycles)	D
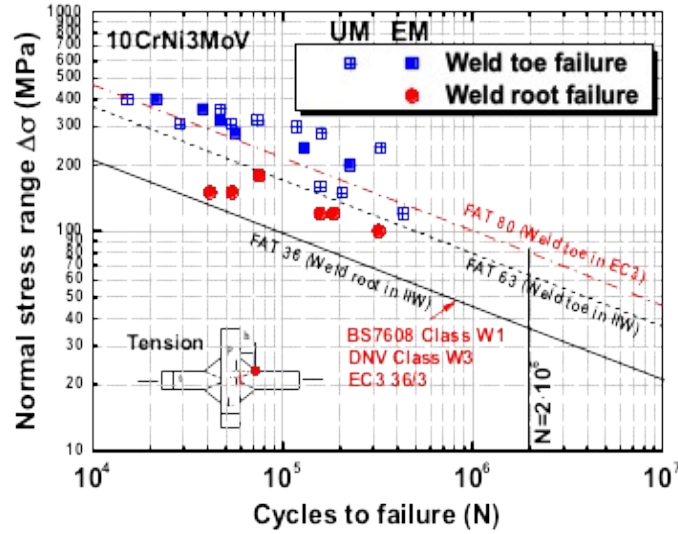
Fig. 4 LCWJ fatigue data of 10CrNi3MoV for weld toe and root failure

4. Fatigue Crack propagation analysis

4.1 Crack propagation model

As it is well known, the total fatigue life of welded joints comprises two major stages. The first is the crack initiation, which belongs to the microstructure growth process. The second is the crack propagation stage in the macro-scale fracture mechanics regime. The total fatigue life can be considered to be the sum of cycles these two periods [32]:

$$N_T = N_I + N_P$$ (3)

Due to the limitation of the Paris law for the short fatigue crack growth stage, it could not accurately describe the SIF variation below the fatigue crack growth threshold. In our study, no limit existed in materials is assumed. Furthermore, the crack propagation fatigue life N_p can be deduced from the Paris law equation:

$$N_p = \int_{a_0}^{a_{cr}} \frac{da}{C(\Delta K_{eff})^m} = \int_{a_0}^{a_{cr}} \frac{da}{C(f(a))^m}$$ (4)

Where a_0 stands for the initial crack length, and a_{cr} is the final critical crack length. C and m are

the material parameters for a specific loading condition. The number of cycles can be calculated by crack extension from the length a_0 to the length a_{cr}.

According to different failure modes in LCWJs, the relevant crack growth parameters of Paris law should be distinguished between a toe-oriented crack propagating into the base metal and a root-oriented crack propagating into the weld deposit metal. Regarding the crack initiation from weld toe, the reference data are derived from the Paris law parameters of base metal in Table 4. In contrast, the material FCGR properties of weldments (EM and UM) were subsequently applied for the weld root-oriented crack. For the sake of comparison with design standards, the related values are used from IIW recommendations, and the material parameters are given to correlate nominal stress data in table 4. Generally, the weld root crack propagation in load-carrying cruciform joints shows mix growth fracture mode. The effective SIF range ΔK_{eff} can be calculated by Tanaka equation in this paper:

$$\Delta K_{eff} = \sqrt[4]{\Delta K_I^4 + 8\Delta K_{II}^4} \tag{5}$$

Where ΔK_I and ΔK_{II} are the SIF ranges in terms of mode I and mode, respectively. The fatigue crack propagation rate is modified according to Eq. 1:

$$da/dN = C \cdot \Delta K_{eff}^m \tag{6}$$

During fatigue crack propagation of weld root, the Kink angle in LCWJs significantly affects SIFs of crack tips. Taking into the combined effects of mode-I and mode-II consideration, crack growth angles can be predicted by Maximum Tangential Stress (MTS) [33] and the maximum Strain Energy Release Rate (SERR) criterion [34]. MTS states the crack growth process from the initial crack tip along the radial direction of tangential stress σ_θ to final fracture. The kink angle θ can be expressed by Eq. 7.

$$\theta = \cos^{-1} \frac{3K_{II}^2 + \sqrt{K_I^4 + 8K_I^2 K_{II}^2}}{K_I^2 + 9K_{II}^2} \tag{7}$$

Finally, these models can be used to explain some phenomena of fatigue crack behavior.

4.2 Fatigue crack propagation simulation

In the simulation process of crack growth, it will be realized by a combination platform of ABAQUS and FRANC 3D. The initial geometry, linear elastic material parameters, boundary conditions, and loading conditions are applied to finite element models of LCWJ in ABAQUS. Models of LCWJ are firstly pre-meshed in ABAQUS. After that, the predefined crack according to actual fractography of fracture surface is inserted into potential failure region and re-meshed the models in FRANC 3D. Then, the combined models will input ABAQUS to calculate stress fields and import them into FRANC 3D to obtain the SIF solutions and other results. ABAQUS is used as a solver to calculate the mechanical response of fatigue crack growth. In the next step, the cruciform joints with crack growth will be updated again in FRANC 3D by an automatic creating crack increment in order to obtain the corresponding stress field surrounding crack in ABAQUS. This procedure is depicted in Fig. 5. It is worth noting that the mixed effect of different loading cases is re-evaluated to recalculate the SIF components in FRANC3D. The crack increment of line and the semi-elliptical crack front is given as follows:

$$\Delta a_{nodei} = \Delta a_{user} \left(\frac{\Delta K_{nodei}}{\Delta K_{eq,mean}} \right)^n \tag{8}$$

A quasi-static analytical pattern is applied to simulate the mix-mode crack propagation step by step for the whole process. It means that SIFs are calculated for each step with crack growth, and the crack shape is modified. Then the crack front mesh is adjusted simultaneously. As for LCWJs, the crack increment of the front point with the mean SIF value ΔK. More techniques about the fatigue crack propagation simulation are illustrated in [19].

The relevant fracture model with crack growth would be performed into ABAQUS and FRANC3D to calculate the crack growth parameters and update the geometry of cruciform joints and mesh them. Consequently, the whole relevant fracture results until the crack grows to a failure length, including stress components, SIFs, kink angles, crack propagation life can be successfully obtained.
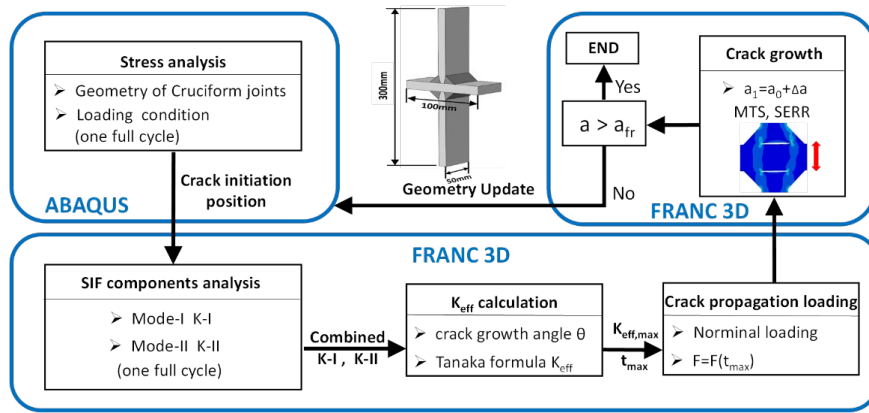
Fig. 5 Simulation procedure of fatigue crack growth

Fig. 6 shows the comparison of fatigue crack propagation routes between experimental observations and prediction results. The simulation weld toe failure path is in accordance with the innovative fatigue crack growth line in Fig. 6(a). As for the fatigue crack initiation from weld root in Fig. 6(b), the simulation crack propagation kink and route are the same as the real fatigue fracture angle and path. It verifies that the calculation procedure of fatigue failure from the weld toe and weld root owns reasonability for one mode and mix-mode crack growth analysis.

As mentioned before, the failure modes in LCWJ can be divided into two modes, weld toe and weld root failure. According to the real fracture surface characteristics of LCWJ in Fig. 6(c) and (d), the crack shape is also classified into two types. One type is line crack occurred at weld toe or root along the specimen width (see Fig. 6(c)) and another type is an elliptical crack that crack initiates from one point of weld toe, then propagates along the elliptical line to failure (see Fig. 6(d)). In light of the difference of fatigue crack propagation shapes, the line and elliptical cracks are employed to investigate the fatigue fracture behavior by combining the material FCGR in the following study. Meanwhile, the fatigue failure boundary with crack growth is defined as a 50% thickness of the plate.
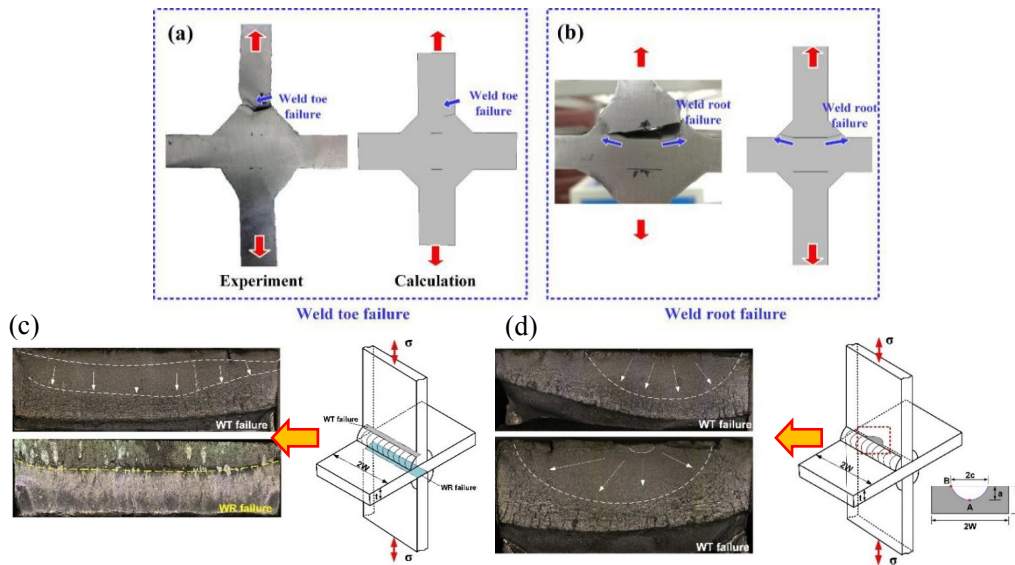
Fig. 6 Fatigue failure routes comparison of LCWJ between experimental and prediction results. (a) Weld toe initiation, (b) Weld root crack initiation, (c) Line crack characteristic, (d) Elliptical crack characteristic.

4.3 Determination of initial crack and analytical models

A small portion of fatigue life for welded joints is spent in crack initiation, which can be neglected in practical engineering structures [11]. It is well known that calculations based on LEEM theory are extremely sensitive to the initial crack. Fatigue crack propagation life prediction of LCWJs is not only strongly dependent upon initial crack position and size but also dependent on the crack types. According to reference, the fatigue failure mode transition range of load-carrying cruciform joints was estimated based on the SED theory, which was about 0.87-1.2 [9]. Therefore, the crack position from weld root or weld toe can be approximately predicted by these analytic solutions. The initial crack size can be found in different recommendations, such as IIW [1], BS7910 [12], Eurocode 3 [13], etc. On the basis of same commendations and specimens fracture characteristics, three types of initial crack shape were investigated in our study, which was semi-elliptical crack (initiated from weld toe or root), single edge line through the crack (Initiated from weld toe) and double edges line through crack (Initiated from weld root). For the semi-elliptical crack, the crack aspect ratio a/2c is used to characterized initial crack shape.

Previous experimental investigations on fatigue life of cruciform joints demonstrated that 0.1mm crack initiation could spend 40% fatigue life for various welding procedures [32]. Other fatigue tests on load-carrying welded joints showed that the cycles of crack growth to 0.5mm oriented from weld root could account for 70% whole life [35]. In the IIW recommendation[1], a correlation between fatigue properties and fracture initial crack size is shown. The initial crack in IIW recommendation is a_i=0.1mm, and the aspect ratio of semi-elliptical is a/c=1.0. During crack propagation, the crack shape variation under specific loading conditions is governed by another two factors, stress gradient, and material properties. The stress gradient is also dependent on component geometry. On the other hand, the accurate computation of crack propagation by fracture mechanics needs base metal and HAZ Paris law material parameters that reflect different

fatigue failure positions.

According to the types of initial crack and the failure locations, the related SIF analytical models have been proposed in some standards or articles. For the line crack initiated from weld toe in LCWJ, the analytical model is given in IIW standard as follows:

$$K = \left[\sigma_m \cdot Y_m(a) \cdot M_{k,m}(a) + \sigma_b \cdot Y_b(a) \cdot M_{k,b}(a)\right] \cdot \sqrt{\pi a} \tag{9}$$

Where the Y stands for structural geometry, and M represents the crack state. σ_m and σ_b are membrane stress and bending stress, respectively. a presents crack size. This formula is usually rewritten to conduct the parameterization study as below:

$$K = M_k \cdot Y \cdot \sigma \cdot \sqrt{\pi a} \tag{10}$$

In this equation, the Mk can be obtained from the following equation:

$$M_k = C \cdot (\frac{a}{T})^k \tag{11}$$

Where:

$$\begin{cases} C = 0.9055 - 0.4369 \cdot (\frac{h}{T}) + 0.1753 \cdot (\frac{h}{T})^2 + 0.0665 \cdot (\frac{w}{T})^2 \\ k = -0.2307 - 0.5470 \cdot (\frac{h}{T}) + 0.2167 \cdot (\frac{h}{T})^2 + 0.2223 \cdot (\frac{w}{T}) \end{cases} \tag{12}$$

Besides, Y is expressed as:

$$Y = 1.12 - 0.38 \cdot (\frac{a}{T}) + 10.6 \cdot (\frac{a}{T})^2 - 21.7 \cdot (\frac{a}{T})^3 + 30.4 \cdot (\frac{a}{T})^4 \tag{13}$$

In contrast, Frank and Fisher[36] carried out finite element experiments to determine the root-oriented crack propagation fatigue life in LCWJs and proposed a corresponding stress intensity factor empirical formula, which was adopted by IIW. It is shown as follows:

$$K_I = \left[\frac{A_1 + A_2\left(2a/w\right)}{1 + 2\left(h/t_p\right)}\right] \cdot \sigma \cdot \sqrt{\pi a \sec\left(\frac{\pi a}{w}\right)} \tag{14}$$

Where the H is the leg length, t_p is plate thickness, A_1 and A_2 are the function as follows:

$$w = H + t_p / 2 \tag{15}$$

$$x = H/t_p \tag{16}$$

$$A_1 = 0.528 + 3.287 \cdot x - 4.361 \cdot x^2 + 3.696 \cdot x^3 - 1.875 \cdot x^4 + 0.415 \cdot x^5 \tag{17}$$

$$A_2 = 0.218 + 2.717 \cdot x - 10.171 \cdot x^2 + 13.123 \cdot x^3 - 7.775 \cdot x^4 + 1.783 \cdot x^5 \tag{18}$$

For a crack in the simple plate, a simplified analytical model is also given to predict SIF in BS 7910 guideline [12], which is similar to Eq.10. If the crack initiates from the weld toe as a line crack shape in a fillet joint, such as Fig. 7(a), Y is considered by the Eq.(19):

$$Y = v\left(\frac{a}{B}\right)^w \left[1.12 - 0.23 \cdot \left(\frac{a}{B}\right) + 10.6 \cdot \left(\frac{a}{B}\right)^2 - 21.7 \cdot \left(\frac{a}{B}\right)^3 + 30.4 \cdot \left(\frac{a}{B}\right)^4\right], 0 < a/B \le 0.6 \tag{19}$$

Where a and B are the crack length and plate thickness in the cruciform joints. v and w are functions of L/B, which can be determined by given values in BS 7910. If the crack initiates from the weld root as a line shape in a fillet joint, such as Fig. 7(a), the equation is expressed as follows, which is similar to Eq. 10:

$$K = M_{km} \cdot f_W \cdot \sigma \cdot \sqrt{\pi a} \tag{20}$$

Where f_w is a finite width correction factor, and M_{km} is geometry correction parameter:

$$f_W = \sqrt{\sec\left[\frac{\pi}{2} \cdot \left(\frac{2a}{W}\right)\right]} \tag{21}$$

$$M_{km} = \lambda_0 + \lambda_1 \cdot \left(\frac{2a}{W}\right) + \lambda_2 \cdot \left(\frac{2a}{W}\right)^2 \tag{22}$$

Where the λ_0, λ_1, λ_2 are given in the following equations:

$$\begin{cases} \lambda_0 = 0.956 - 0.343 \cdot \left(\frac{h}{T}\right) \\ \lambda_1 = -1.219 + 6.210 \cdot \left(\frac{h}{T}\right) - 12.220 \cdot \left(\frac{h}{T}\right)^2 + 9.704 \cdot \left(\frac{h}{T}\right)^3 - 2.741 \cdot \left(\frac{h}{T}\right)^4 \\ \lambda_2 = 1.954 - 7.938 \cdot \left(\frac{h}{T}\right) + 13.299 \cdot \left(\frac{h}{T}\right)^2 - 9.541 \cdot \left(\frac{h}{T}\right)^3 + 2.513 \cdot \left(\frac{h}{T}\right)^4 \end{cases} \tag{23}$$

Regarding as the elliptical crack, the Eq. can be rewritten to this formula:

$$K = M_{km} \cdot f_W \cdot \sigma \cdot \sqrt{\pi a / Q} \tag{24}$$

where: $\qquad Q = 1 + 1.464 * (a/c)^{1.65} \tag{25}$

Finally, The SIF analytical solutions from IIW and BS 7910 guidelines are compared to verify the accuracy of numerical results for different crack types, and fatigue propagation life is further assessed by fracture mechanics theory considering various factors, such as geometry and misalignment.

5. Fatigue results by fracture mechanics approach

5.1 Stress intensity factors

The LCWJ geometry and line initial crack effect on SIFs at weld toe are depicted in Fig.7. Fig. 7(a) shows the effect of initial crack size on SIFs of weld toe with crack growth for the weld geometry case of h=6mm and p/t=0.3. It is shown that the initial crack length has no influence on the SIF values with crack growth. Although SIFs is fixed under specific crack size in weldment, the fatigue life is varied with the modification of initial crack sizes according to the Eq. 4. Additionally, SIFs from calculated results achieve a satisfactory prediction compared with IIW analytical results, especially within the crack growth range of 2 mm. Fig. 7(b) presents the variation of SIFs with weld length under p/t=0.3. The simulation results exhibit consistency with IIW analytical solutions for different weld length. The LCWJs with high penetration length can provide an accurate assessment of SIFs under different line initial crack sizes.

The related simulation data under different initial cracks and weld lengths for the case of h=6mm and p/t=0 are shown in Fig.7(c) and (d). The initial crack seems to be no effect on the SIFs with crack growth. However, a large deviation can be found between the simulation results and IIW analytical solutions for full penetration (p=0mm) in Fig. 7(c). Specifically, the SIF numerical solutions with fatigue crack growth are larger than that of IIW. With the decreases of weld length in the range from h/t=0.5 to h/t=1, the SIFs are gradually decreasing and reach the same level with IIW solutions in Fig. 7(d). When the weld length ratio h/t increases from 0.5 to 1, potential failure location can transfer from weld root to weld toe. Therefore, the IIW analytical solutions

can give a relatively accurate and conservative prediction of SIFs for LCWJ.
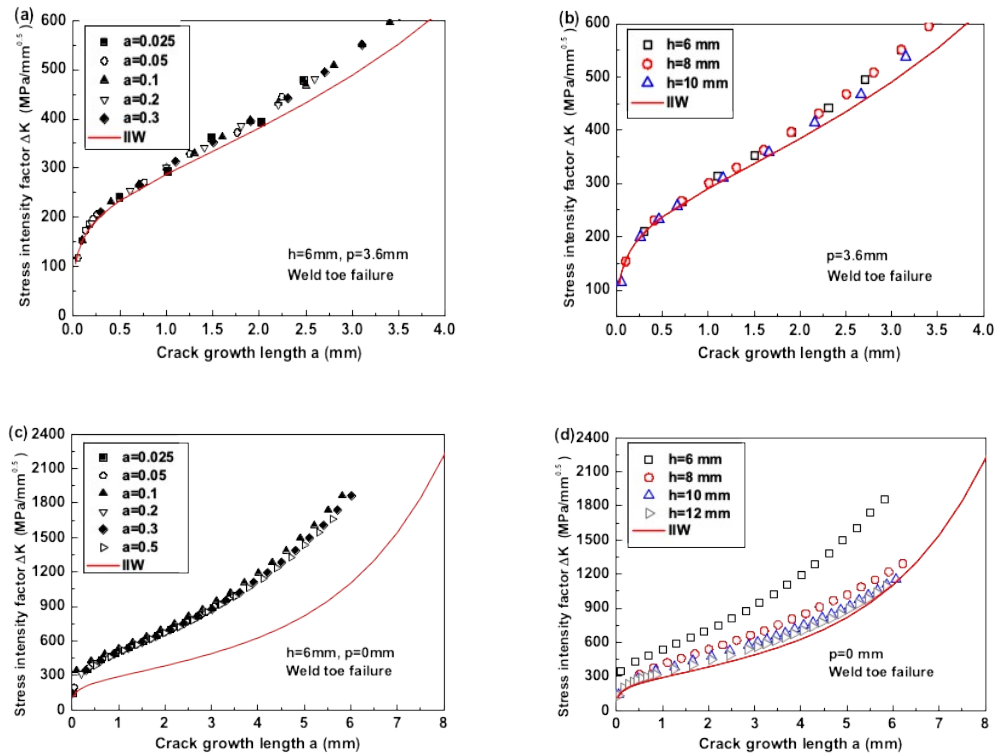
Fig. 7 SIFs of weld toe for FCG in LCWJ under p/t=0.3 and p/t=0. (a) Weld length 6 mm at p/t=0.3; (b) Different weld length effect at p/t=0.3; (c) Weld length 6 mm at p/t=0; (d) Different weld length effect at p/t=0

Regarding the weld root failure, the SIF comparisons between numerical and analytical solutions are given considering different initial crack sizes and weld lengths in Fig. 8. Note that similar to the results of SIFs at weld toe, the line initial crack length has no influence on the SIFs with crack propagation under the combination of h/t=0.5 and no penetration, which is presented in Fig. 8(a). Though the analytical solution of IIW is generally consistent with that of BS7910, the simulation results are larger than standard solutions. Actually, the crack deflection occurs during real crack propagation. Whereas, the crack growth is assumed along a straight line in terms of the calculation procedure from standard solutions. This can be attributed to the extending path deflection during the crack propagation. In Fig. 8(b), the fatigue crack growth driving force decreases with increases of weld length, which leads to enhance the load-carrying capability of welded joints. It is interesting that the difference between numerical results and BS7910 solutions decreases when the weld length size ratio (h/t) increases from 0.5 to 1.
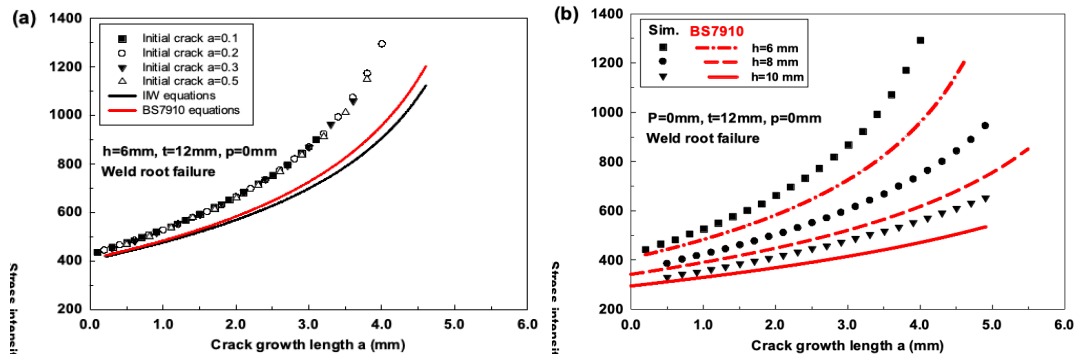
Fig. 8 SIFs at weld root for FCG in LCWJ under p/t=0. (a) Weld length 6 mm; (b) Weld length effect

To further reveal the effect of penetration length, three related geometry sizes (P/T=0, P/T=0.1, P/T=0.2) are selected by comparing the variations of SIFs under specific weld geometries (h/t=0.5 and h/t =0.67). It is clearly observed from Fig. 9 that SIFs decrease with the increases in penetration size. Particularly, no penetration length can lead to the largest deviation between simulation and BS7910 results. The results of standard solutions are less than the numerical solutions, which means a prediction of longer fatigue life can be obtained. Thus, the standard solutions give a conservative reference line for fatigue life assessment. When the penetration size ratio P/T reaches to 0.2, the two solutions under both h/t=0.5 and h/t =0.67 conditions give good agreement.
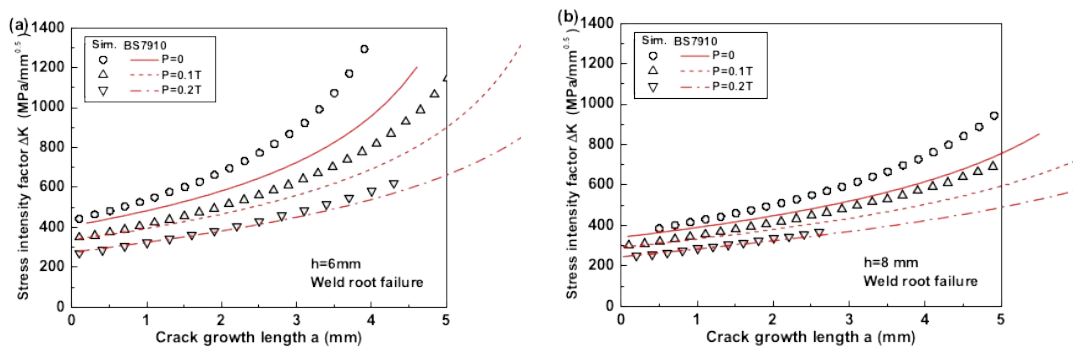
Fig. 9 SIFs of WR for FCG in LCWJ due to weld length and penetration size. (a) Weld length 6 mm; (b) Weld length 8 mm

On the other hand, an initial semi-elliptical crack is introduced at the weld toe on the base plate. According to the IIW recommendations, the initial semi-elliptical crack size is adopted as a/c=0.5, a=0.1mm. Without considering the effect of HAZ fracture properties, furthermore, the base metal is set as calculated material fracture parameters. Refined meshes around the crack tip are generated automatically. A comparison among the line crack calculated results, and elliptical crack calculated results and IIW analytical solutions are provided in Fig. 10. Similar to the fatigue crack growth simulation of line crack, the SIFs of an elliptical crack is lower than that of line crack. It should be emphasized that the initial crack plane is parallel to the plate thickness direction along the weld toe.
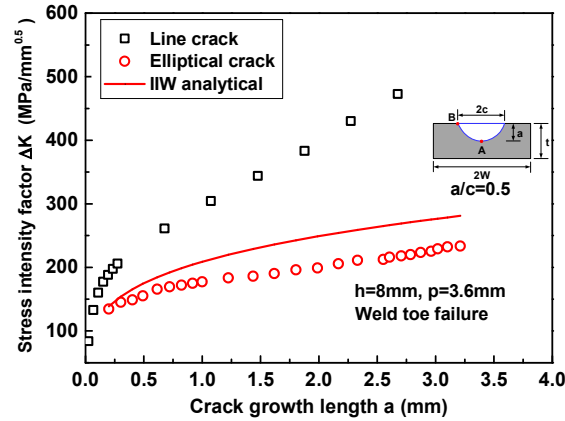
Fig. 10 SIFs of different crack types

Accurate fatigue life prediction depends on the accurate a-K relationship. The fatigue crack growth life can be estimated from the above calculation results. The different FCG properties of base metal and weldments can be ascribed to the microstructure discrepancy. For specific fatigue failure locations, the fatigue crack propagation life can be estimated according to Paris parameters. Therefore, it is important to determine the fatigue failure mode in LCWJ by performing the SIFs analyses. Generally, the fatigue crack orientated from weld toe, the parameters of base metal are chosen. By contrast, the weldment parameters are employed for the fatigue crack initiated from the weld root.

As we all know, fatigue life will decrease with increasing crack depth. In order to quantitatively characterize the relationship between fatigue life and initial crack size, the fatigue life of LCWJ can be determined directly according to failure location. Herein the initial crack depth is taken as 0.025 mm and 0.2 mm. 100MPa nominal loading (σ_m) is applied in the model. Finally, the a-N curves are depicted in Fig for different initial crack.

Fig. 11(a) shows the difference of fatigue life for weld toe failure considering the Paris parameters of BM, UM, EM, and IIW under different penetration lengths. The fatigue life of BM is longest in the same initial geometry and loading conditions, while the UM parameters give shortest fatigue growth life, which is comparative with IIW parameters. Regarding the 0.2mm initial crack, a similar tendency with Fig. 11(a) are demonstrated in Fig. 11(b). As mentioned before, the fatigue life based on 0.2mm initial crack is not much lower than that of 0.075 initial cracks. In terms of penetration length effect, the fatigue life under p/t=0 in Fig. 11 is shorter than that under p/t=0.3 about 2 to 3 times by comparing it with Fig. 11. Thus, there is no magnitude order variation for crack propagation life considering penetration size.
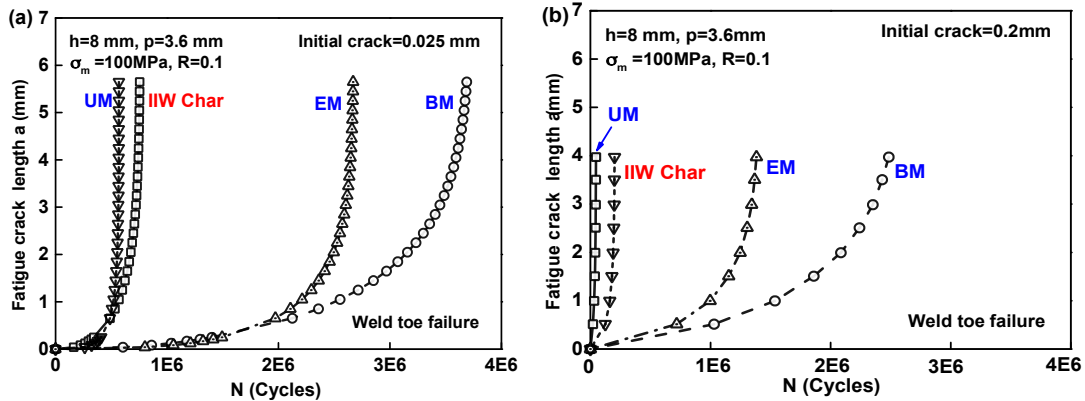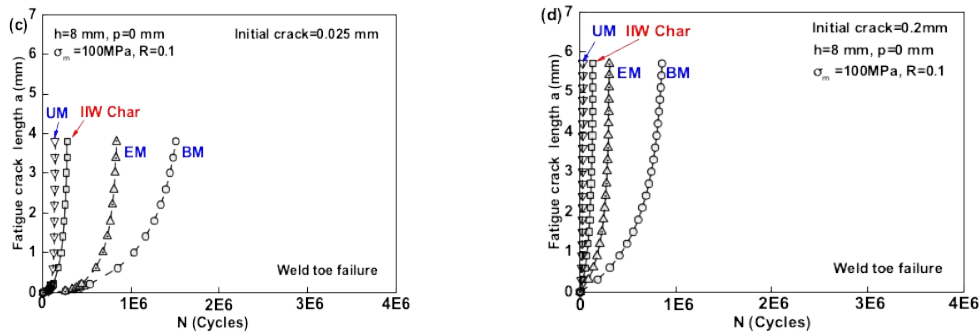
Fig. 11 WT fatigue life curves of different materials and initial linear crack length considering the penetration effect (P/t=0.3 and P/t=0). (a) Initial crack length 0.025 mm; (b) Initial crack length 0.2 mm

Fig. 12 presents the test results, predicted S-N curves of LCWJs corresponding to specific fatigue details and the standard reference lines. FAT 63/3 is selected as the standard reference line of fatigue life assessment for Weld Toe (WT) failure. In Fig. 12(a), the predicted S-N curves (gray lines) based on IIW fracture mechanics parameters decline with the increases of initial crack sizes. Predicted results under a = 0.2 mm can almost approach the IIW reference line. Fig. 12(b) demonstrates the predicted S-N results considering BM fracture parameters. The calculated fatigue propagation life of LCWJs is overestimated compared with the real fatigue life data. The crack propagation analysis using the evenmatched (EM) weldment fracture parameters predict the fatigue life of LCWJ in good agreement with the evenmatched LCWJ test data (solid blue square) for a=0.025mm from Fig. 12(c). Due to the higher FCGR of undermatched weldments than other materials, the predicted fatigue life by UM fracture parameters is lower than the IIW reference line and real fatigue life data in Fig. 12(d).

Overall, comparisons between the predicted curves and test data show that the combination of a=0.025mm and EM fracture parameters can provide an accurate prediction of EM LCWJs. To involve most of the fatigue test data, we suggest that the a=0.2mm is used to calculate the fatigue life as the initial crack.
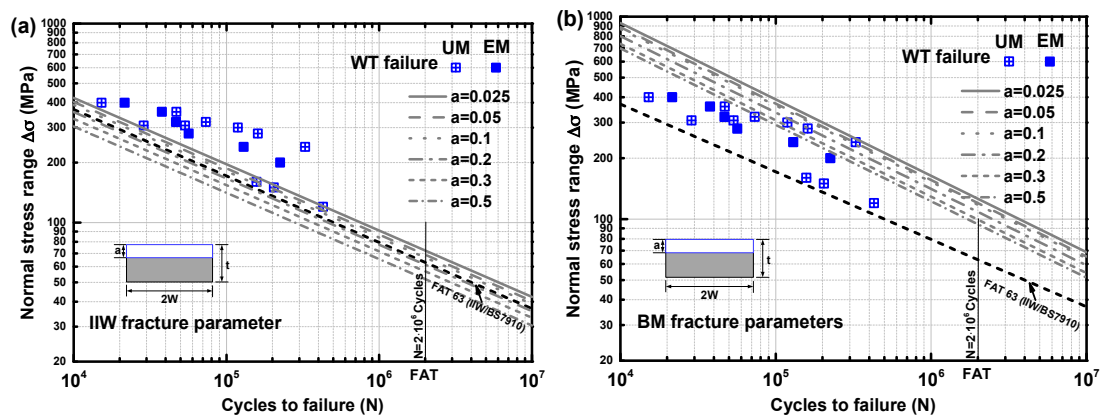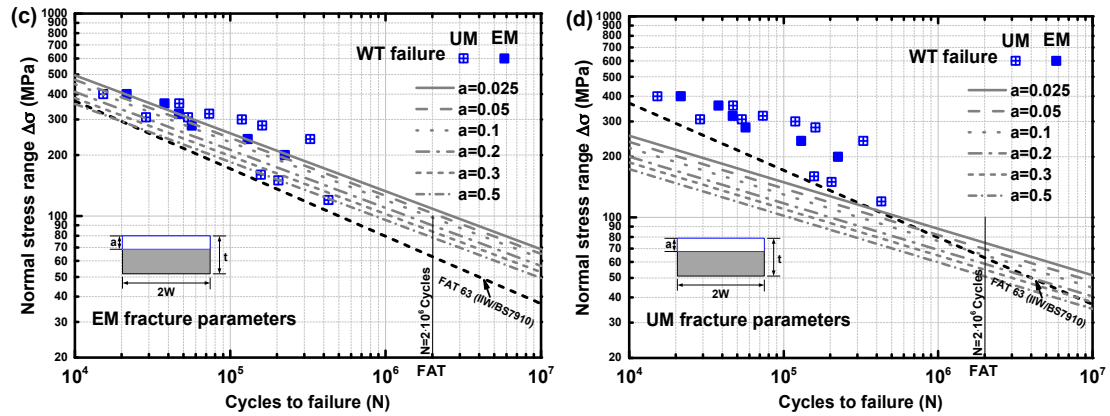
Fig. 12 Weld toe S-N curves of different materials and initial crack length. (a) IIW fracture parameters; (b) BM fracture parameters; (c) EM fracture parameters(d); UM fracture parameters

Fig. 13 compares the test results, the standard reference lines, and predicted S-N curves of LCWJs considering the semi-elliptical crack for WT failure. Though the IIW fracture parameters give conservative fatigue life prediction for initial line crack, the estimates from the IIW parameters for semi-elliptical crack exhibits are comparable with the test data from Fig. 13(a). The fatigue life predicted lines under other material parameters were also analyzed and presented in Fig. (b), (c) and (d), respectively. The results show that the predicted lines from the BM and EM fracture parameters give overestimated tendency, while the S-N lines from UM fracture parameters demonstrate conservative estimations in Fig. 13(d).

Based on the above analysis, it is found that the Paris fracture parameters have great influences on fatigue life compared with the effect of the initial crack size. On the other hand, the line crack can exert lower fatigue life curves by fracture mechanics theory than the semi-elliptical crack. In summary, from the perspective of predictive reliability, the line initial crack a=0.2mm and IIW fracture parameters are recommended to assess the weld toe failure for 10CrNi3MoV LCWJs.
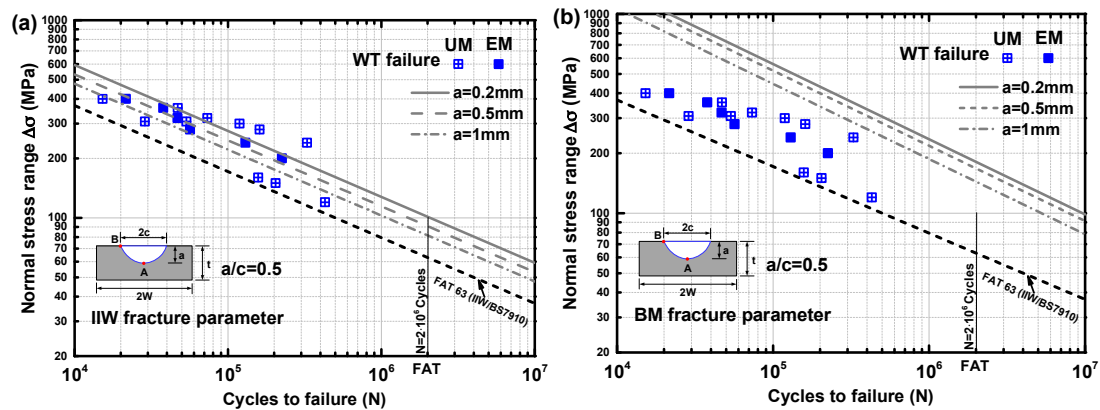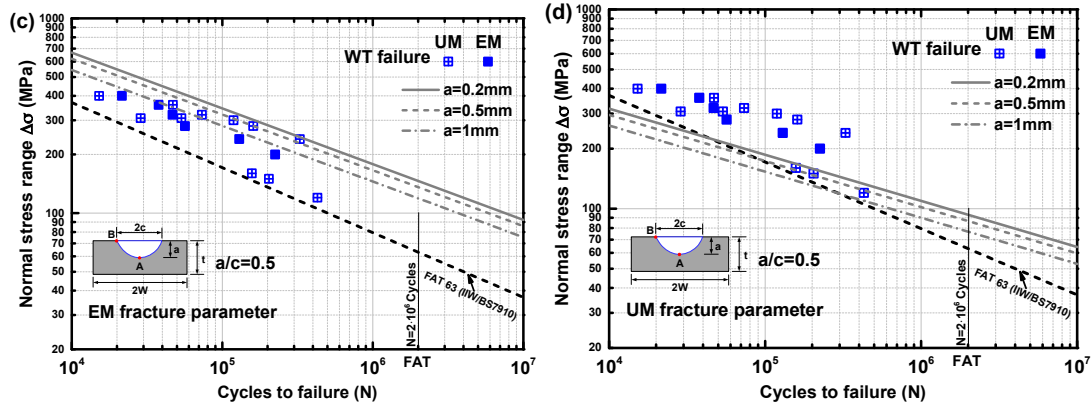
Fig. 13 WT S-N curves of different materials and initial elliptical crack length. (a) IIW fracture parameters; (b) BM fracture parameters; (c) EM fracture parameters; (d) UM fracture parameters

According to the real fracture graph of the weld root in Fig. 14(a), the line initial crack is adopted to compute the fatigue crack growth life. The results comparison of fatigue life under different fracture parameters and weldment geometries for weld root failure is presented in Fig. 14. The line initial crack size seems to be a negligible effect on the S-N curves. From the SIFs calculations before, the corresponding predicted S-N curves based on IIW and UM parameters are lower than the test data of evenmatched LCWJs. Fortunately, the crack propagation analysis using the EM FRGR results with a=0.1mm can provide a proximate prediction of the fatigue life for EM LCWJs. Fig. 14(d) shows the effect of weld length on predicted S-N curves. The fatigue failure from weld root demonstrates higher fatigue life with the increases of the weld length. It is because the intensity of LCWJs load-carrying enhances and further the introduced increases of the fatigue crack growth resistance are beneficial to prolong the fatigue failure from weld root.

Similarly, the predicted S-N curves considering the penetration effect, are shown in Fig. 14(e) and (f). Three penetration ratios (p/T=0, 0.1, 0.2) are given. Predicted fatigue lives of LCWJs under IIW and EM fracture parameters had a favorable effect of penetration length within the range 0-0.2. The significant increase in fatigue life also can be attributed to the lower SIFs under larger penetration length. The EM parameters combined with P/T=0 can give an accurate prediction of fatigue life.
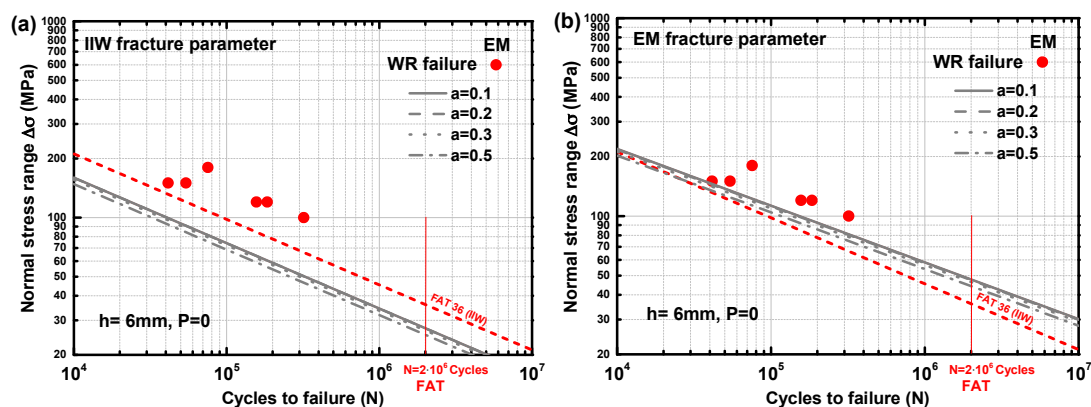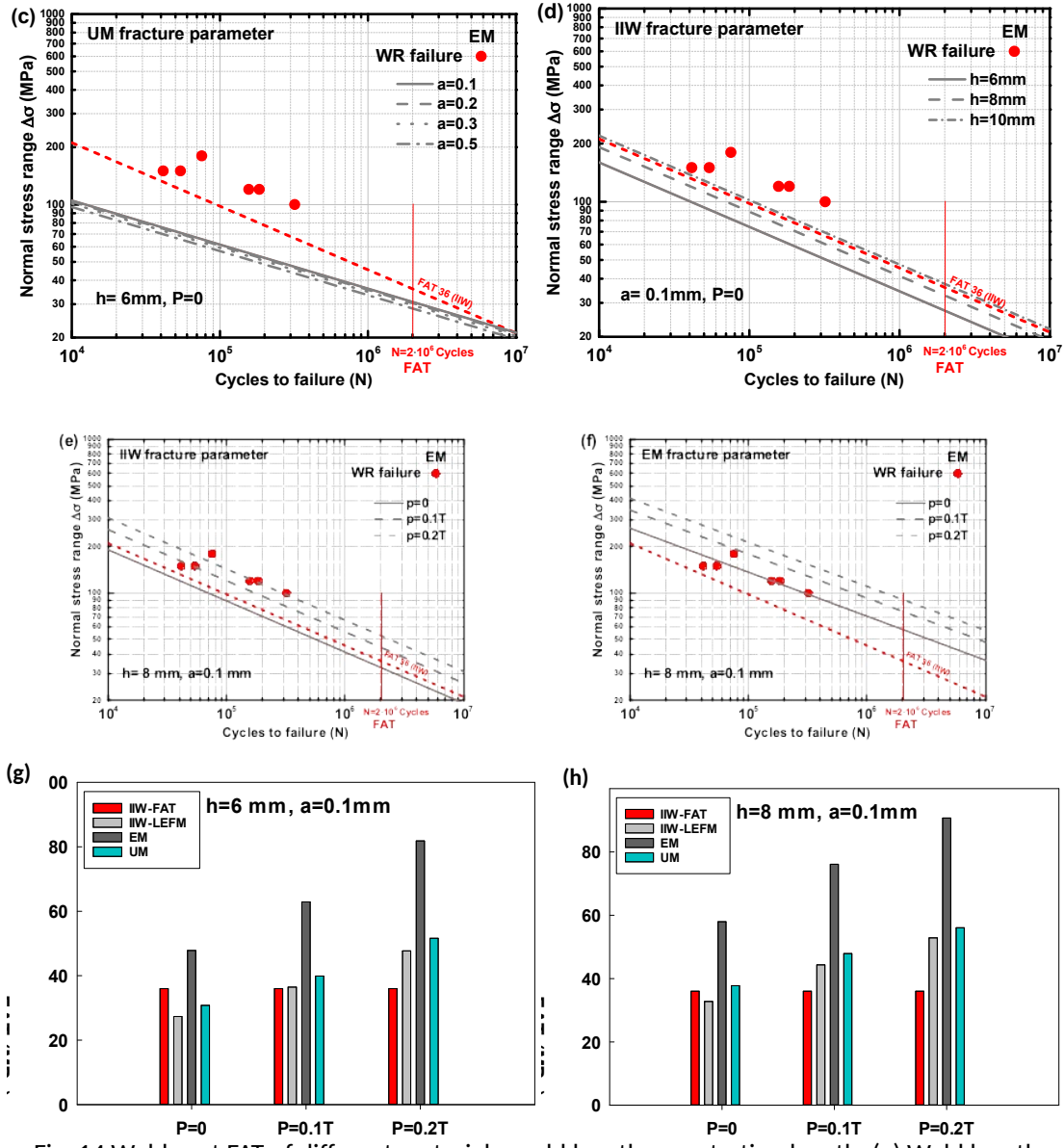
Fig. 14 Weld root FAT of different materials, weld length, penetration length. (a) Weld length h/t=0.5; (b) Weld length h/t=0.67

Fig. 14 The S-N curves evaluation for weld root failure considering different material parameters and weld geometries. (a) Different initial crack sizes under IIW fracture parameters; (b) Different initial crack sizes under EM fracture parameters; (c) Different initial crack sizes under UM fracture parameters; (d) Different weld lengths under IIW fracture parameters; (e) Different penetration lengths under IIW fracture parameters; (f) Different weld lengths under EM fracture parameters; (g) Weld root FAT for Weld length h/t=0.5 under different penetration ratio; (h) Weld root FAT for Weld length h/t=0.67 under different penetration ratio

To investigate the fatigue strength at $2*10^6$ cycles under different penetration ratio and material fatigue fracture discrepancy, the corresponding FAT values are extracted and compared from the predicted S-N curves considering the specific initial crack size in Fig. 14(g) and (h). In this section, the initial line cracks size a=0.1 is assumed. Compared with IIW recommendation FAT values, the predicted FAT values from IIW weldment fracture parameters are much more acceptable for weld root failure than other material fracture parameters in both cases of weld length (h/t=0.5 and h/t=0.67). The determination of the safe S-N boundary reference line is of great significance for the discreteness of fatigue test data. Based on the above analysis, the weld

root failure under the combination of a=0.1, P/t=0, and h/t=0.5 can give a conservative lower S-N reference line, which is almost coincidence with IIW FAT36 curve.

6. Conclusion:

The fatigue performance of LCWJ has been studied in this paper. FCGR tests for base metal and weldments are conducted. 3D mix-mode fatigue crack growth simulation was developed by interaction application of ABAQUS and Franc 3D software based on fracture mechanics theory. Furthermore, the comparison between the predicted and experimental fatigue lives was carried out. The following conclusions can be proposed based on the results:

(1) The FCGR of 10CrNi3MoV base metal is faster than that of evenmatched and undermatched weldments within the ΔK range of 55 MPa$\cdot$m^2. Above this value, the FCGR of base metal slower than WM and UM weldments.

(2) The influences of initial crack shape, initial crack size, and material fracture properties on fatigue fracture behavior of LCWJs were explored. The relationships between initial cracks and SIFs were assessed by comparison with the standards' analytical solution. The calculated SIFs initial line crack at weld toe location was in accordance with BS7910 analytical solutions, while the BS7910 results at weld root were lower than the calculation results due to lacking consideration of crack growth deflection.

(3) In terms of LCWJ fatigue life test data, the data of evenmatched LCWJs shows no significant difference with that of undermatched LCWJs. Besides, the Eurocode 3 design curves are not suitable for weld toe failure of UM LCWJ specimens. It is better to choose the IIW standards for LCWJ fatigue life assessment.

(4) The fatigue life prediction based on fracture mechanics theory for weld toe and weld root failure were analyzed. Parametric analysis for different initial crack and joint geometry was conducted. The weld length has a slight influence on the fatigue life for both failure modes. Otherwise, the penetration size exhibits a significant effect on fatigue life, which determines the final failure mode. Signal semi-elliptical crack seems to give a non-conservative estimation. It proved that 0.2mm initial line crack combined with the IIW fracture parameter was recommended for weld toe failure in LCWJ. In contrast, the initial line crack does not affect the fatigue life of the weld root. Thus, no penetration length, 0.1 mm initial line crack, and weldments fracture parameters can provide the basic S-N curve prediction for weld root failure.

Statements of Contribution

Acknowledgements :

References:

1.   Hobbacher AF. Recommendations for Fatigue Design of Welded Joints and Components, IIW Collection. *Recommendations for Fatigue Design of Welded Joints and Components.* 2016.

2.   Kainuma S, Mori T. A study on fatigue crack initiation point of load-carrying fillet welded cruciform joints. *International Journal of Fatigue.* 2008;30(9):1669-1677.

3.   Kainuma S, Mori T. A fatigue strength evaluation method for load-carrying fillet welded cruciform joints. *International Journal of Fatigue.* 2006;28(8):864-872.

4.   Xing S, Dong P, Threstha A. Analysis of fatigue failure mode transition in load-carrying fillet-welded connections. *Marine Structures.* 2016;46:102-126.

5.   Lazzarin P, Tovo R. A notch intensity factor approach to the stress analysis of welds. *Fatigue and Fracture of Engineering Materials and Structures.* 1998;21(9):1089-1103.

6.   Lazzarin P, Livieri P, Berto F, Zappalorto M. Local strain energy density and fatigue strength of welded joints under uniaxial and multiaxial loading. *Engineering Fracture Mechanics.* 2008;75(7):1875-1889.

7.   Meneghetti G, Marini D, Babini V. Fatigue assessment of weld toe and weld root failures in steel welded joints according to the peak stress method. *Welding in the World.* 2016;60(3):559-572.

8.   Xing S, Dong P, Wang P. A quantitative weld sizing criterion for fatigue design of load-carrying fillet-welded connections. *International Journal of Fatigue.* 2017;101:448-458.

9.   Song W, Liu X, Berto F, Wang P, Xu J, Fang H. Strain energy density based fatigue cracking assessment of load-carrying cruciform welded joints. *Theoretical and Applied Fracture Mechanics.* 2016.

10.   Verreman Y, Limodin N. Fatigue notch factor and short crack propagation. *Engineering Fracture Mechanics.* 2008;75(6):1320-1335.

11.   Hobbacher AF. Comparison of fatigue verification procedures at a thick-walled welded component. *Welding in the World.* 2017;61(4):801-818.

12.   British Standard I. BS-7910 - Guide to methods for assessing the acceptability of flaws in metallic structures. *BS 7910 Guide to Methods for Assessing the Acceptability of Flaws in Metallic Structures.* 2005.

13.   European Committee for S. EN 1993-1-9 Eurocode 3. *Design of Steel Structures - Part 1-9: Fatigue.* 2005.

14.   Nykänen T, Marquis G, Björk T. A simplified fatigue assessment method for high quality

welded cruciform joints. *International Journal of Fatigue*. 2009;31(1):79-87.

15. Fischer C, Fricke W, Rizzo CM. Review of the fatigue strength of welded joints based on the notch stress intensity factor and SED approaches. *International Journal of Fatigue*. 2016;84:59-66.

16. Fricke W, Gao L, Paetzold H. Fatigue assessment of local stresses at fillet welds around plate corners. *International Journal of Fatigue*. 2017;101:169-176.

17. Zong L, Shi G, Wang YQ, Li ZX, Ding Y. Experimental and numerical investigation on fatigue performance of non-load-carrying fillet welded joints. *Journal of Constructional Steel Research*. 2017;130:193-201.

18. Su H, Wang J, Du J. Fatigue behavior of uncorroded non-load-carrying bridge weathering steel Q345qDNH fillet welded joints. *Journal of Constructional Steel Research*. 2020;164:105789.

19. Zong L, Shi G, Wang Y-Q, Yan J-B, Ding Y. Investigation on fatigue behaviour of load-carrying fillet welded joints based on mix-mode crack propagation analysis. *Archives of Civil and Mechanical Engineering*. 2017;17(3):677-686.

20. Liu Y, Tsang KS, Hoh HJ, Shi X, Pang JHL. Structural fatigue investigation of transverse surface crack growth in rail steels and thermite welds subjected to in-plane and out-of-plane loading. *Engineering Structures*. 2020;204.

21. Chapetti MD, Steimbreger C. A simple fracture mechanics estimation of the fatigue endurance of welded joints. *International Journal of Fatigue*. 2019;125:23-34.

22. Ahola A, Björk T, Barsoum Z. Fatigue strength capacity of load-carrying fillet welds on ultra-high-strength steel plates subjected to out-of-plane bending. *Engineering Structures*. 2019;196.

23. Wang B, Nagy W, De Backer H, Chen A. Fatigue process of rib-to-deck welded joints of orthotropic steel decks. *Theoretical and Applied Fracture Mechanics*. 2019;101:113-126.

24. Lepore M, Berto F. On the fatigue propagation of multiple cracks in friction stir weldments using linear and non-linear models under cyclic tensile loading. *Engineering Fracture Mechanics*. 2019;206:463-484.

25. Chernyatin AS, Matvienko YG, Razumovsky IA. Fatigue surface crack propagation and intersecting cracks in connection with welding residual stresses. *Fatigue and Fracture of Engineering Materials and Structures*. 2018;41(10):2140-2152.

26. Steimbreger C, Chapetti MD. Fatigue strength assessment of butt-welded joints with undercuts. *International Journal of Fatigue*. 2017;105:296-304.

27. Leitner M, Barsoum Z, Schäfers F. Crack propagation analysis and rehabilitation by HFMI of pre-fatigued welded structures. *Welding in the World*. 2016;60(3):581-592.

28. Lewandowski J, Rozumek D. Cracks growth in S355 steel under cyclic bending with fillet welded joint. *Theoretical and Applied Fracture Mechanics*. 2016;86:342-350.

29. Song W, Liu X, Berto F, Razavi SMJ. Low-Cycle Fatigue Behavior of 10CrNi3MoV High Strength Steel and Its Undermatched Welds. *Materials*. 2018;11(5).

30. E647 A. Standard test method for measurement of fatigue crack growth rates. 2013.

31. Song W, Liu X, Razavi SMJ. Fatigue assessment of steel load-carrying cruciform welded joints by means of local approaches. *Fatigue & Fracture of Engineering Materials & Structures*. 2018;41(12):2598-2613.

32. Lassen T. The effect of the welding process on the fatigue crack growth. *Welding Journal*. 1990;69(2):75S-81S.

33. Erdogan F, Sih GC. On the crack extension in plates under plane loading and transverse shear. *Journal of Basic Engineering*. 1963;85:519-527.

34. Sih GC. Strain-energy-density factor applied to mixed mode crack problems. *International Journal of Fracture*. 1974;10(3):305-321.

35. Lazzarin P, Livieri P. Notch stress intensity factors and fatigue strength of aluminum and steel welded joints. *International Journal of Fatigue*. 2001;23(3):225-232.

36. Fisher JW, Frank KH, Hirt MA. NCHRP Report 102: Effect of Weldments on the Fatigue Strength of Steel Beams. 1970.